Crystal Structure Analysis of the Activation of Histidine by *Thermus thermophilus* Histidyl-tRNA Synthetase[†,||]

A. Åberg,[‡] A. Yaremchuk,[‡] M. Tukalo,[§] B. Rasmussen, and S. Cusack*

European Molecular Biology Laboratory, Grenoble Outstation, c/o ILL 156X, 38042 Grenoble, France

Received July 24, 1996; Revised Manuscript Received October 24, 1996[⊗]

ABSTRACT: The crystal structure at 2.7 Å resolution of histidyl-tRNA synthetase (HisRS) from *Thermus thermophilus* in complex with its amino acid substrate histidine has been determined. In the crystal asymmetric unit there are two homodimers, each subunit containing 421 amino acid residues. Each monomer of the enzyme consists of three domains: (1) an N-terminal catalytic domain containing a six-stranded antiparallel β-sheet and the three motifs common to all class II aminoacyl-tRNA synthetases, (2) a 90-residue C-terminal α/β domain which is common to most class IIa synthetases and is probably involved in recognizing the anticodon stem−loop of $tRNA^{His}$, and (3) a HisRS-specific α-helical domain inserted into the catalytic domain, between motifs II and III. The position of the insertion domain above the catalytic site suggests that it could clamp onto the acceptor stem of the tRNA during aminoacylation. Two HisRS-specific peptides, 259-RGLDYY and 285-GGRYDG, are intimately involved in forming the binding site for the histidine, a molecule of which is found in the active site of each monomer. The structure of HisRS in complex with histidyl adenylate, produced enzymatically in the crystal, has been determined at 3.2 Å resolution. This structure shows that the HisRS-specific Arg-259 interacts directly with the α-phosphate of the adenylate on the opposite side to the usual conserved motif 2 arginine. Arg-259 thus substitutes for the divalent cation observed in seryl-tRNA synthetase and plays a crucial catalytic role in the mechanism of histidine activation.

The fidelity of protein biosynthesis is dependent on the correct charging of tRNAs with their cognate amino acids. This reaction, which occurs in two steps, is catalyzed by the aminoacyl-tRNA synthetases (aaRSs) which specifically recognize both the amino acid and its cognate tRNA(s) as well as the ATP required for the initial amino acid activation [for reviews see Cusack (1995) and Delarue (1995)]. These enzymes are divided into two distinct classes which are distinguishable on the basis of sequence comparisons as well as three-dimensional structure (Eriani *et al.,* 1990; Cusack *et al.,* 1990). The catalytic domain of class I aaRSs comprises a five-stranded parallel β-sheet with connecting helices, referred to as the nucleotide binding (Rossmann) fold, which is also found in a number of functionally unrelated enzymes. Class II enzymes have a catalytic domain built around a six-stranded antiparallel β-sheet (Cusack *et al*., 1990), a similar fold having been identified only in biotin synthetase (Artymiuk *et al*., 1994). In class I aaRS the conserved, class-defining, sequence motifs KMSKS and HIGH are responsible for the interaction with the universal substrate ATP and for assisting catalysis, whereas in class II synthetases it is residues of the so-called motifs 2 and 3 that play this role, notably an absolutely conserved arginine from each motif. Another class II defining motif, motif 1, characterized by an almost conserved proline, is responsible for dimer interactions in class II aaRS.

The three-dimensional structures of 11 different synthetases have been determined (Cusack *et al*., 1995): from class I, MetRS (Brunie *et al.,* 1990) and GlnRS from *Escherichia coli* (Rould *et al.,* 1989), GluRS from *Thermus thermophilus* (Nureki *et al*., 1995), and TyrRS (Brick *et al.,* 1989) and TrpRS (Doublié *et al.,* 1995) from *Bacillus stearothermophilus*, and from class II, SerRS from both the *E. coli* and *T. thermophilus* systems (Fujinaga *et al.,* 1993), HisRS from *E. coli* (Arnez *et al.,* 1995), GlyRS from *T. thermophilus* (Logan *et al.,* 1995), AspRS from both *Saccharomyces cerevisiae (*Ruff *et al.,* 1991) and *T. thermophilus* (Delarue *et al*., 1994; Poterszman *et al*., 1994), LysRS from both *E. coli* (Onesti *et al.,* 1995) and *T. thermophilus* (Cusack *et al.,* 1996b), and PheRS from *T. thermophilus* (Mosyak *et al.,* 1995). Structural information for the synthetase in complex with its cognate tRNA is available for the Glu (Rould *et al.,* 1989), Asp (Ruff *et al.,* 1991), Ser (Biou *et al.,* 1994; Cusack *et al*., 1996a), and Lys systems (Cusack *et al.,* 1996b).

The structural basis of amino acid and ATP recognition and the mechanism of activation have been described in detail for the class II aspartyl- (Cavarelli *et al*., 1994) and seryl- (Belrhali *et al*., 1995) enzymes and the class I glutaminyl- (Perona *et al*., 1994) enzyme. Differences in the observed magnesium binding sites in the case of the two class II synthetases suggest that different enzymes might differ in detail in their active centers (Belrhali *et al*., 1995).

Histidyl-tRNA synthetase is one of smallest class II aminoacyl-tRNA synthetases with an homodimeric structure and subunit molecular mass of about 47 kDa in prokaryotic systems. A number of distinctive features make the histidyl system of particular interest. It is classified as a member of subclass IIa primarily because of the presence of a putative

[†] The research of M.T. was supported in part by an International Research Scholar's award from the Howard Hughes Medical Institute.

[||] Coordinates have been deposited in the Brookhaven Protein Data Bank under entry codes ladj and lady for the *T. thermophilus* histidyl-tRNA synthetase complexed with histidine and with histidyl adenylate, respectively, and are available on request from cusack@embl-grenoble.fr.

* Corresponding author: Tel (33) 4-76-20-72-38; FAX (33) 4-76-20-71-99.

[‡] Joint first authors.

[§] Also affilitated with the Institute of Molecular Biology and Genetics, 252627 Kiev, Ukraine.

[⊗] Abstract published in *Advance ACS Abstracts,* February 15, 1997.

S0006-2960(96)01837-5 CCC: $14.00

anticodon binding C-terminal domain which is homologous to that of threonyl-, prolyl-, and some glycyl-tRNA synthetases (Cusack *et al.*, 1991; Cusack, 1995). On the other hand, sequence alignments show it to be otherwise distinct from other class IIa synthetases (Cusack *et al*., 1991). In particular, there are two peptides preceding motif 3 (RGLDYY and GGRYDGL) which are highly conserved in all known HisRS sequences, the second of which is also found in the histidyl-tRNA synthetase-like domain of yeast GCN2 (Wek *et al*., 1989).

Histidine-specific tRNAs are unique for the additional guanosine (designated G-1) present at their 5′ end, giving rise through pairing with the discriminator base (C73 in prokaryotes and organelles, A73 or G73 in eukaryotes) to an extra base pair in the acceptor stem (Steinberg *et al*., 1993). As shown by *in vitro* aminoacylation of transcripts, the G-1·C73 base pair in *E. coli* is the most important determinant for HisRS (Himeno *et al*., 1989). Furthermore, minihelices corresponding to the acceptor stem and TΨC loop of $tRNA^{His}$ are efficiently aminoacylated by HisRS (Franklyn & Schimmel, 1990; Franklyn *et al.*, 1992). More recently, *in vivo* studies have shown that the identity of histidine tRNAs in *E. coli* depends more on C73 than G-1 (Yan *et al.*, 1994). On the other hand, in the yeast histidyl system, the exact nature of the additional base pair seems less important (except that G73 is a strong negative determinant), suggesting that the major recognition elements may be the extra backbone groups at the 5′ end (Nameki *et al.*, 1995). As far as specific recognition of the GUG anticodon goes, *in vitro* results suggest that in the *E. coli* system the anticodon bases are weak identity elements whereas in the yeast system bases 34 and 35, but not 36, are relatively more important (Nameki *et al.*, 1995). The manner of binding of the C-terminal domain of class IIa synthetases to the anticodon stem−loop is one of the remaining open structural questions about this subclass of synthetases.

We have previously reported the purification and cocrystallization of HisRS from *T. thermophilus* (HisRSTT) with histidine (Yaremchuk *et al.*, 1995). Here we describe the structure of the HisRSTT−histidine complex determined at 2.7 Å resolution which reveals the overall architecture of the enzyme as well as details of the recognition of the amino acid substrate. In addition, we have determined the structure of the complex of HisRSTT with histidyl adenylate at 3.2 Å resolution, obtained after soaking the original crystals with Mn^{2+} and ATP.

The two structures reported here show high similarity to that of the *E. coli* HisRS complexed with histidyl adenylate (Arnez *et al*., 1995). The particularly new information provided by this work comprises (a) the sequence and structure of a thermostable HisRS, (b) visualization of the insertion domain, disordered in the *E. coli* HisRS structure, and (c) based on the structures of the histidine complex and the histidyl adenylate complex formed *in situ* by addition of ATP, a more complete structural description of the activation step.

MATERIALS AND METHODS

Cloning and Sequencing of T. thermophilus HisRS. The *hisS* gene of *T. thermophilus* HisRS has been isolated from genomic DNA obtained from *T. thermophilus* HB 27 cells. The amino acid sequence of the N-terminal 43 residues, determined by protein sequencing, together with highly conserved regions of HisRS was used to define several oligonucleotides as primers for PCR. Two oligonucleotides, corresponding to the first six N-terminal residues and a conserved heptapeptide in the central part of protein, were used to select a single DNA fragment of 850 bp by means of the PCR (Yaremchuk *et al.*, unpublished results). That this corresponded to a putative HisRS gene was verified by cloning and DNA sequencing. The cloned fragment was then used as a probe for Southern blot hybridization to *T. thermophilus* chromosomal DNA digested with several restriction enzymes. A 2.5 kb *Hin*dIII/*Bam*HI fragment was cloned into pUC18 plasmid and sequenced using the dideoxynucleotide method (Sanger *et al.*, 1977). The open reading frame of the *hisS* gene contains 1263 bp, from which the sequence of the 421 amino acid residues comprising the subunit was deduced.

Crystallization. Crystals of histidyl-tRNA synthetase were grown from protein purified from *T. thermophilus* using ammonium sulfate as precipitant, with the substrate histidine present in the crystallization solution (Yaremchuk *et al.*, 1995). The crystals belong to the space group $P2_12_12$ with cell dimensions $a = 171.3$ Å, $b = 214.7$ Å, $c = 49.3$ Å, and $\alpha = \beta = \gamma = 90°$. There are four monomers per asymmetric unit and approximately 45% of the crystal volume is occupied by solvent.

Diffraction Measurements. Data on the native crystals were collected on the high brilliance beamline ID2 (BL4) at the European Synchrotron Radiation Facility (ESRF) using a 30 cm Mar-Research image plate detector. A complete native data set to 2.7 Å resolution was collected on a single flash-frozen crystal at 100 K using a 0.7° rotation to avoid spot overlap. The exposure time was 20 s per image. The data are essentially complete with an R_{sym} on intensities of 5% (Table 1).

Heavy atom derivatives obtained using compounds containing Hg, Au, U, and Pb were used to determine the HisRS structure. Native crystals were soaked 24 h in solutions of the mother liquor containing either 1 mM $HgCl_2$, 1 mM $KAuCl_4$, 1 mM uranyl acetate, or 20 mM trimethyllead acetate, respectively. Data were collected to 4 Å resolution for the U and Pb soaked crystals and to 2.9 Å for the Au and Hg soaked crystals. All data were collected at ID2 (BL4), ESRF. Typical exposure times were 10−20 s/deg.

Two independent data sets, respectively on beamline ID9 (BL3) and beamline ID2 (BL4) at the ESRF, have been collected on single crystals which prior to freezing were soaked for 30 min in mother liquor containing 10 mM ATP and 10 mM Mn^{2+}. The data are of poorer quality than the native due to crystal deterioration upon soaking but are complete to 3.2 Å resolution with some data to 2.8 Å in the ID9 data collection (Table 1).

Structure Determination. All processing was done using the CCP4 program package (1994). The structure of HisRS was determined by the method of multiple isomorphous replacement (MIR). The mercury sites were located by both automated (RSPS) and manual Patterson techniques and refined with MLPHARE. The resulting phases were used to determine the heavy atom positions in the other derivatives by difference Fourier methods. The MIR phases, calculated with all four derivatives, had an overall mean figure of merit of 0.62 for the centric reflections and 0.40 for the acentric for data in the resolution range 20−3 Å. Phases were improved by solvent flattening and 4-fold averaging using

Table 1: Data Collection and Phasing Statistics

crystal	native	ATP + Mn^{2+}		Hg	Au	U	Pb
		A	B				
resolution (Å)	2.7	2.8	3.2	2.9	2.9	4.1	4.1
no. of reflections							
unique	49630	32840	28929	36732	34311	12895	12812
total	214739	85481	70515	109395	94228	34497	38390
completeness (%)[a]	99 (95)	65 (30)	93.6 (85.5)	88 (59)	75 (65)	87 (51)	90 (50)
R_{sym}[b] (%)	5.0	9.0	9.8	4.9	5.3	2.8	4.3
R_{der}[c] (%)				13	15	18	20
phasing power[d]				0.70	1.36	0.66	0.69
no. of sites				4	7	4	6

[a] Numbers in parentheses for completeness designate values for the highest resolution shell. [b] $R_{sym} = \Sigma|I - \langle I\rangle|\Sigma I$, where I = observed intensity and $\langle I\rangle$ = average intensity for multiple measurements. [c] $R_{der} = \Sigma||F_{PH}| - |F_P||/\Sigma|F_P|$, where $|F_{PH}| - |F_P|$ are the heavy atom derivative and protein structure factor amplitudes, respectively. [d] Phasing power = rms($|F_H|/E$), where $|F_H|$ = heavy atom structure factor amplitude and E = residual lack of closure error. Data were indexed and integrated with the programs IPMOSFLM (Leslie, 1992) or DENZO (Otwinowski, 1993). All data were collected on ESRF beamline ID2 except collect A on ATP + Mn^{2+} which was collected on ID9.

Table 2: Refinement Statistics

	histidine complex	histidyl adenylate complex
resolution limits (Å)	20−2.7	20−2.8
R-factor (%) (no. of reflections)	21.7 (46757)	26.0 (31181)
R_{free} (no. of reflections)	27.7 (2502)	30.0 (1632)
no. of amino acid residues	4 × 420	4 × 420
no. of water molecules	283	0
no. of sulfate ions	4	4
no. of ligands	4 × histidine	4 × histidyl adenylate
av protein *B*-factor (Å^2)	38	38
av ligand *B*-factor (Å^2)	30	40
RMS bond deviations (Å)	0.010	0.006
RMS angle deviations (deg)	1.497	1.184

the program DM. Maps calculated at 3 Å resolution with solvent-flattened MIR phases clearly showed the characteristic β-sheet of class II synthetases. All model building was done using the program O (Jones *et al.*, 1995).

Refinement of the Histidine Complex. The initial model had an R_{cryst} of 0.48 for all data. The structure was refined using X-PLOR (Brünger, 1993) with the protein parameters defined by Engh and Huber (1991). Initially, strict noncrystallographic constraints between the four monomers were used. After several rounds of simulated annealing, positional refinement, and rebuilding, tight noncrystallographic restraints (except for restricted regions) were used instead of strict non-crystallographic constraints. During the final stages of refinement water molecules were inserted into the model using peaks in the $F_o - F_c$ maps. Waters with *B*-factors above 80 Å^2 were excluded from the model. Solvent corrections were included during the refinement as implemented in X-PLOR using a small solvent radius of 0.25 Å. The course of the refinement was checked by the 5% of reflections left out from the beginning and used to calculate an R_{free}. The final model has an R_{factor} of 22.0% and $R_{free}$of 27.7% using all data to 2.7 Å resolution. This model comprises 4 × 420 residues (the N-terminal methionine is not visible), 283 water molecules, four histidines, and four sulfate ions (Table 2). The Ramachandran plot for the final model shows that more than 91% of the residues are in the most favored regions and that only two residues, in poorly ordered zones, are in disallowed regions.

Refinement of the Histidyl Adenylate Complex. The refined model of the HisRSTT−histidine complex, but with the histidine and all water molecules removed, was used as the starting point for the refinement of the histidyl adenylate complex. After rigid-body refinement and positional refinement with tight geometrical and NCS restraints, difference maps showed clear density for the histidyl adenylate (Figure 3b), the reordered motif 2 loop, and other small changes. Inclusion of histidyl adenylate in the model, but not water molecules, led to a current *R*-factor (R_{free}) of 26% (30%) (see Table 2).

RESULTS

Sequence and Overall Structure of T. thermophilus HisRS. The primary structure of HisRSTT that we have derived from the gene sequence is shown in Figure 1 aligned to five other prokaryotic HisRS. The *T. thermophilus* enzyme is composed of 2 × 421 amino acid residues with a total molecular mass of 96 kDa. HisRSTT is 37% identical in sequence to the corresponding enzyme from *E. coli* whose structure is already known (Arnez *et al*., 1995).

The structure of HisRSTT was solved by multiple isomorphous replacement using four heavy atom derivatives (Table 1). The asymmetric unit contains two complete dimers which was used to improve the electron density maps by 4-fold averaging of the electron density. Using the primary structure of HisRSTT which we have derived from the gene sequence, a model has been refined with X-PLOR (Brunger, 1991) at 2.7 Å resolution using noncrystallographic restraints. The final model shows good stereochemistry with an overall R = 22% and R_{free} = 28% for all reflections. Further details are given in Materials and Methods and Tables 1 and 2.

The overall structure of a monomer and dimer of HisRSTT is shown in Figure 2, and the derived secondary structure is superposed on the sequence alignment in Figure 1. The structure is very similar to that already described for the same enzyme from *E. coli* (Arnez *et al*., 1995; see Figure 1 in this paper for a schematic diagram of the secondary structure). The HisRSTT subunit contains three domains: the catalytic domain common to all class II synthetases, the C-terminal domain most likely involved in binding the tRNA anticodon stem−loop, and a third α-helical domain inserted into the catalytic domain between motifs 2 and 3. The C-terminal domain is connected to the catalytic domain via an extended chain of nine residues (321−329). In the dimer, the C-terminal domain of one subunit makes interactions exclusively with the catalytic domain of the other subunit (Figure 2b).

The Catalytic Domain. The catalytic domain, residues 2−171 and 229−320, is based around a seven-stranded

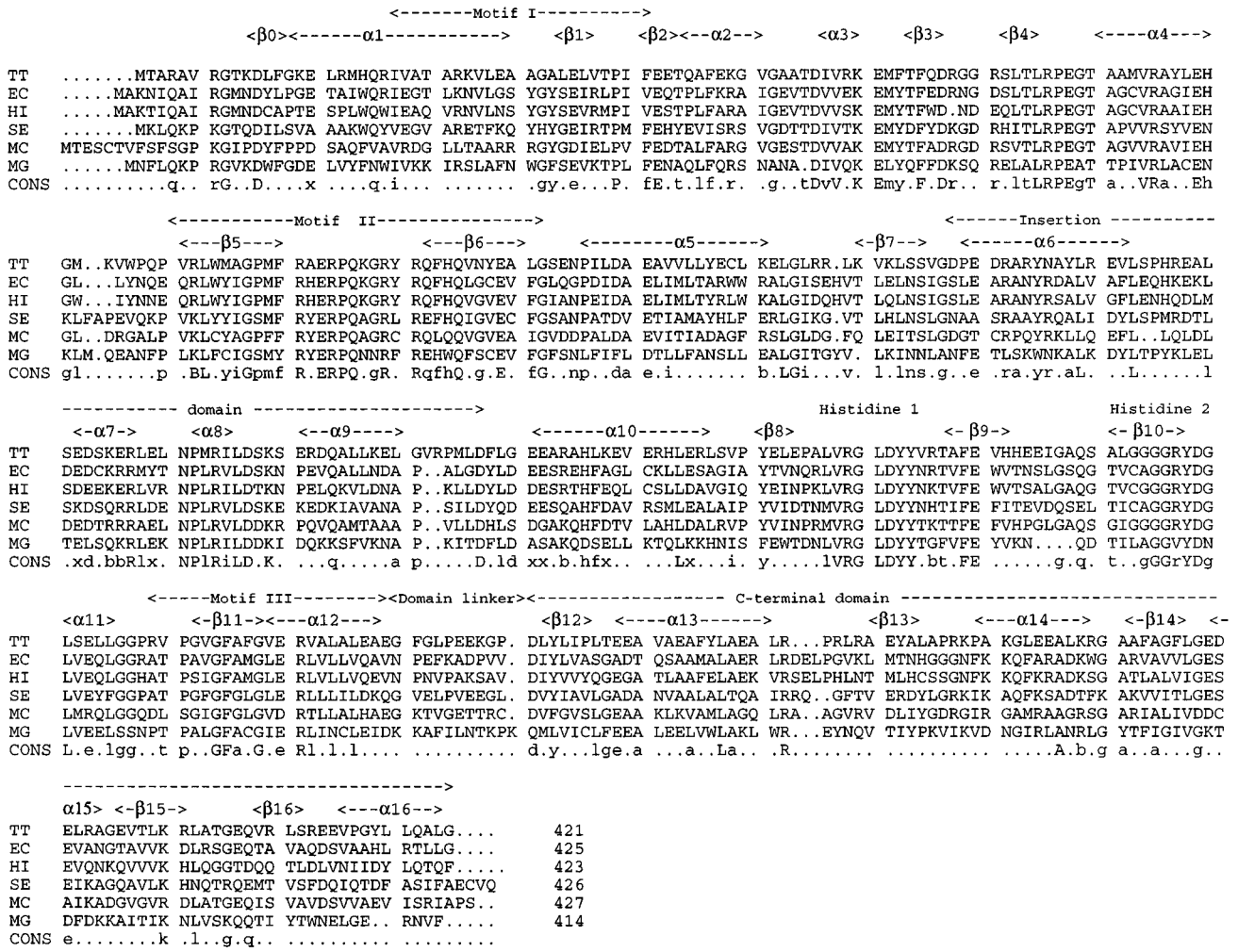

FIGURE 1: Alignments of six prokaryotic histidyl-tRNA synthetase sequences with superposed secondary structure designations for *T. thermophilus* HisRS which were defined according to Kabsch and Sander (1983). In the consensus sequence, capital letters imply full conservation, and small letters imply conservation in four out of six. B(b) is used for lysine or arginine and X(x) for aspartate or glutamate. Abbreviations and SWISSPROT accession numbers are as follows: EC, *E. coli* (P04804); HI, *Hemophilus influenzae* (P43823); SE, *Streptococcus equisimilus* (P30053); MC, *Mycobacterium leprae* (P46696); MG, *Mycoplasma genitalium* (P46220).

β-sheet, six of the strands being antiparallel (β5, β6, β11, β10, β9, β7), surrounded by three long α-helices, the normal class II interface (α1) and crossover (α5) helices and an extra helix (α6) specific for HisRS which is involved with the interface with the C-terminal domain (see below). The six antiparallel strands form the basis for the class II catalytic domain. The seventh β-strand (β8) is parallel to β7 in HisRSTT, which is also the case for class IIb synthetases (AspRS, LysRS) but not SerRS where this strand is antiparallel and can be considered as part of the N-terminal extension of that synthetase.

The Subunit Interface. There are two major components to the intersubunit interface, first, between the two catalytic domains, and second, between the C-terminal domain of one subunit and the catalytic domain of the other. The interface between the two catalytic domains is mediated as in other class II synthetases by the N-terminal part of the catalytic domain including notably motif 1. An intersubunit sheet is formed by β0 making two hydrogen bonds with the antiparallel strand β1′ (where the prime indicates the second subunit), and although the antiparallel loop formed by β3 and β4 crosses over toward the other subunit close to the dimer 2-fold axis, there are, surprisingly, no intersubunit hydrogen bonds with the corresponding loop in the other subunit (β3′ and β4′), thus not forming the cross-subunit four-stranded antiparallel β-sheet as is the case in most other class II synthetases described. Furthermore, in HisRSTT the axes of the long interface helices (α1) of motif 1, antiparallel about the dimer 2-fold axis, are 17 Å apart, too far for their side chains to interact directly as occurs in seryl-tRNA synthetase or class IIb synthetases where the helix axis separation is respectively about 12 and 10 Å. The only interhelix bridging interaction is by Arg-28 on one helix interacting with Glu-38 on the loop after the same helix which in turn interacts with Gln-21′ on the symmetry-related helix. The consequence is that between these two helices, penetrating the dimer, there is a deep solvent-filled crevice which includes a very well-defined sulfate ion bound to each interface helix by Arg-18 and Arg-22. The floor of the crevice is formed by a more substantial hydrophobic interface between the subunits as described for the similar HisRSEC [see Figure 3 in Arnez *et al*. (1995)]. In this region there is a close connection between the two active sites via the highly conserved motif 1 proline-42, similar to that described in detail for the aspartyl system (Eriani *et al*., 1993). The extreme N-terminus of HisRSTT (residues 2−5) also packs on the symmetry-related subunit (Figure 1b) making two inter-subunit hydrogen bonds.

The two subunits are also held together by the C-terminal domain of one subunit which has an extensive interface with

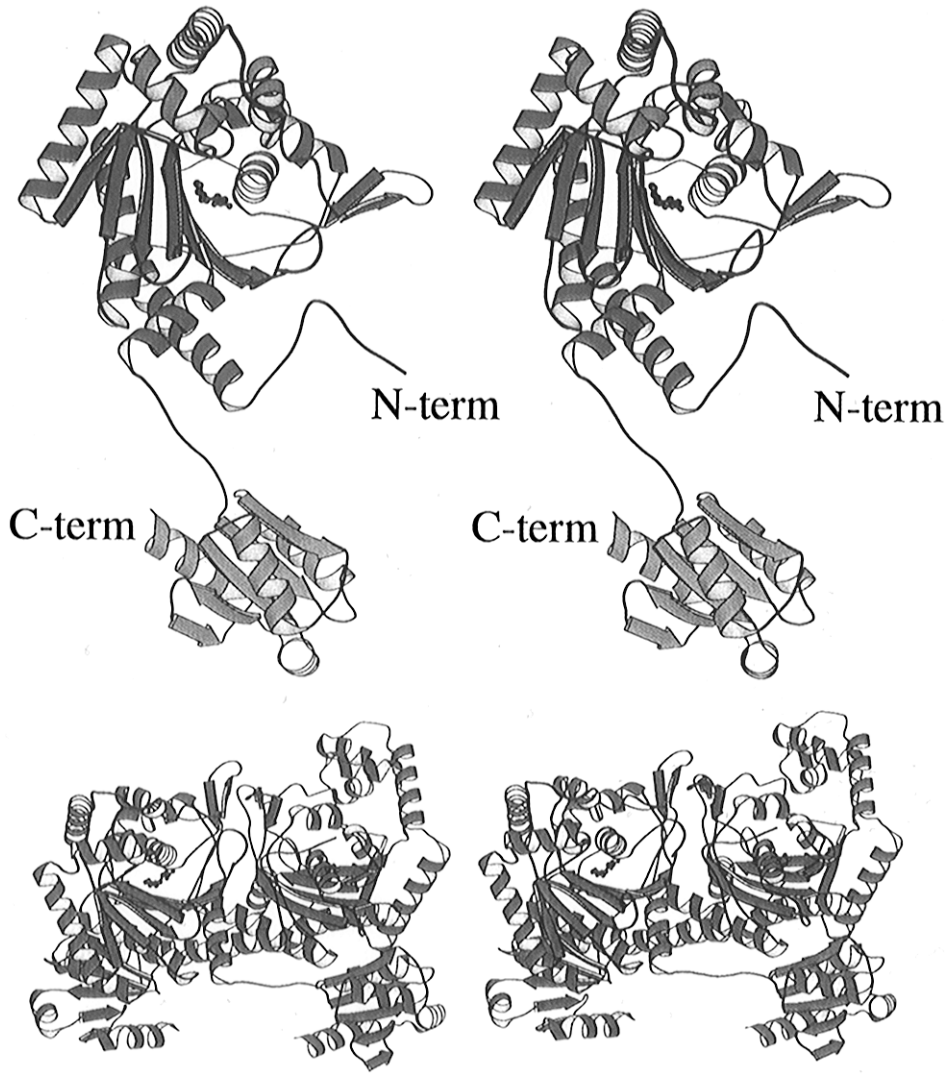

FIGURE 2: Stereoviews of (a, top) one monomer with the histidine substrate, showing the catalytic domain (red), insertion domain (green), and C-terminal domain (blue), and (b, bottom) complete dimer with subunits respectively in red and green.

the catalytic domain of the other subunit. This interaction is mediated by the first helix (α13) and following strand (β13) of the C-terminal domain which pack against the C-terminal end of the interface helix (α1), the crossover helix (α5), and the C-terminal end of the extra catalytic domain helix (α6). The crossover helix is in fact parallel to the first helix (α13) of the C-terminal domain, and the two interact for instance by means of respectively Glu-142′ and Arg-352, both residues being highly conserved in all HisRS sequences.

The Histidine Binding Site. Crystals of HisRSTT could only be grown in the presence of histidine, present in the crystallization medium at a concentration of 5 mM. The solvent-flattened MIR maps show a well-defined electron density at the active site corresponding to a bound histidine which is present in all four monomers (Figure 3a).

The active site of HisRS is overall similar in arrangement to other class II synthetases of known structure although there are several significant differences in detail (Figure 4). Residues fulfilling their expected function are the conserved arginines of motif 2 and motif 3, respectively Arg-112 and Arg-311, and the conserved Phe-124 which stacks with the adenine ring of the adenylate (see below). The motif 2 loop, residues 115−120, is poorly ordered in the presence of the histidine only, consistent with the fact that in other class II synthetases it has been shown to be stabilized only by interactions with the adenine ring of the ATP or adenylate [e.g., Belrhali *et al*. (1994)] and/or with the tRNA (Cusack *et al*., 1996). Features specific to HisRSs are the particular construction of the histidine-binding pocket and the residues found at the α-phosphate catalytic center (see section on adenylate). The histidine binding pocket is formed by two highly conserved peptides, denoted histidine-1 and histidine-2 in Figure 1. The first sequence, histidine-1 (258-VR-GLDYY) makes a loop between β8 and β9 that covers the active site and forms the roof of the histidine binding pocket (Figure 4). In other class II synthetases this loop does not cover the active site to such an extent and the residues do not interact with the substrate. The second HisRS specific sequence (283-GGGGRYDG) forms a β-strand under the histidine substrate ending with Tyr-288, whose side chain forms the side of the histidine pocket. Tyr-288 occupies the structurally equivalent position as the critical glutamic acid (arginine) recognizing the lysine (aspartic acid) in respectively LysRS (Onesti *et al.*, 1995) and AspRS (Poterszman *et al*., 1994). The glycine-rich strand under the histidine is unusual in that though it is part of an antiparallel β-sheet, it is virtually unpleated with all ϕ,ψ angles within $180 \pm 16°$. The second two glycines are conserved in all HisRS, in particular Gly-285 being essential to avoid a steric

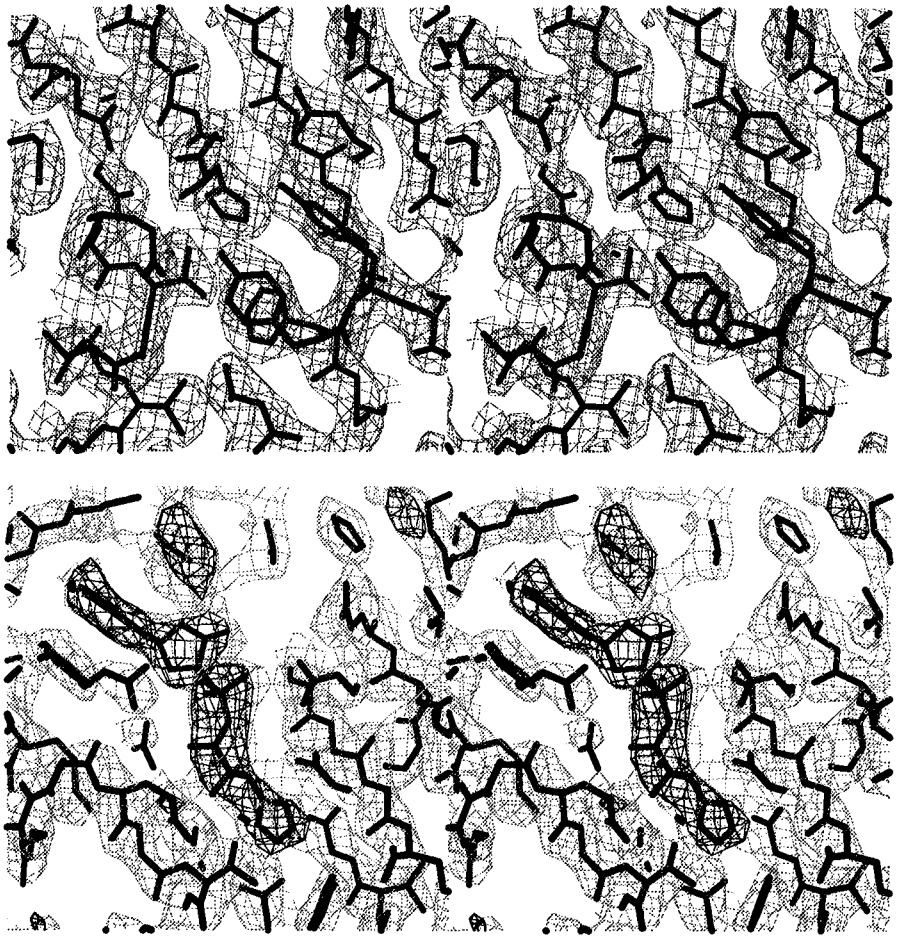

FIGURE 3: (a, top) Experimental electron density for the histidine binding site obtained using MIR phases, solvent flattening, and 4-fold averaging with the superposed final model. The contour level is 1σ, and the substrate histidine is in the center of the figure. (b, bottom) Electron density and final model for the ATP-Mn^{2+} soaked crystal obtained after refinement without histidyl adenylate in the model. The $2F_o - F_c$ map (contour level 1σ) is in dotted lines, and the $F_o - F_c$ map (contour level $+3\sigma$) is in solid black lines. Note the elongated positive difference density at the top center of the image which could be due to released pyrophosphate.

clash with the substrate histidine. In the histidine-2 peptide, the highly conserved Arg-287 and Asp-289 form a salt bridge on the other side of the main chain to Tyr-288 and thus help to lock the correct backbone conformation. Arg-287 also interacts closely with Asp-140, a highly conserved residue in the crossover helix α5. The only current exception to the absolute conservation of these two residues is in HisRSMG where the equivalent residues are respectively valine and phenylalanine, suggesting that hydrophobic interactions have replaced electrostatic interactions at this point in HisRSMG (Figure 1).

Details of the interaction of the enzyme with the substrate histidine are shown in Figures 4a and 5a. The pocket in which histidine binds is highly polar with an extensive array of hydrogen bonds which prevent any hydrophobic amino acid from binding. Histidine specificity is ensured by Glu-130 (motif 2) and Tyr-264 (histidine-1) which form hydrogen bonds respectively to the NE2 and ND1 positions of the histidine ring. Glu-130 is positioned by hydrogen bonds with Asn-128 and Tyr-288. Similarly, Arg-259 can hydrogen bond to the carboxyl group of the amino acid substrate as well as hydrogen bonding to and positioning Tyr-264. This implies that the ND1 of the substrate is deprotonated in order to be a hydrogen bond acceptor for the hydroxyl hydrogen of Tyr-264. These residues form part of a very striking chain of hydrogen-bonded residues extending right across the active site and comprising Ser-280/His-272/Glu-270/Arg-259/Tyr-264. The absolutely conserved residues Glu-81 and Thr-83 from the "TXE loop" (for HisRS, this is in fact an "EGT" loop) common to all class II synthetases (Belrhali *et al*., 1994) both play important roles. Thr-83 interacts with the histidine N-terminus while Glu-81 makes a stabilizing hydrogen bond with Tyr-263, which also interacts with the histidine N-terminus.

Comparison of the active sites of HisRSTT and HisRSEC (Arnez *et al.*, 1995; Figure 6c) shows some minor differences in the substrate interactions between the two enzymes. Residues that differ in the hydrogen bonding between the two structures are *(E. coli* numbering in brackets) Glu-81 (83), Thr-83 (85), Tyr-263 (263), and Asn-128 (Gly-129). These differences may reflect the fact that the HisRSTT complex is with histidine, the HisRSEC complex being with histidyl adenylate (although adenylate formation does not change these interactions in HisRSTT; see below) or, more likely, the species difference that HisRSTT has an extra active site interacting residue (Asn-128 which replaces Gly-129 in HisRSEC).

C-Terminal Domain. HisRSTT contains a C-terminal domain of about 90 residues (330−421) connected to the catalytic domain via a extended chain of 9 residues and very similar to that found in *E. coli* HisRS (Arnez *et al*., 1995). It is a five-stranded mixed β-sheet, with three flanking α-helices and a fourth short helix (α15) in the turn between antiparallel strands β14 and β15 (Figures 1 and 2). As

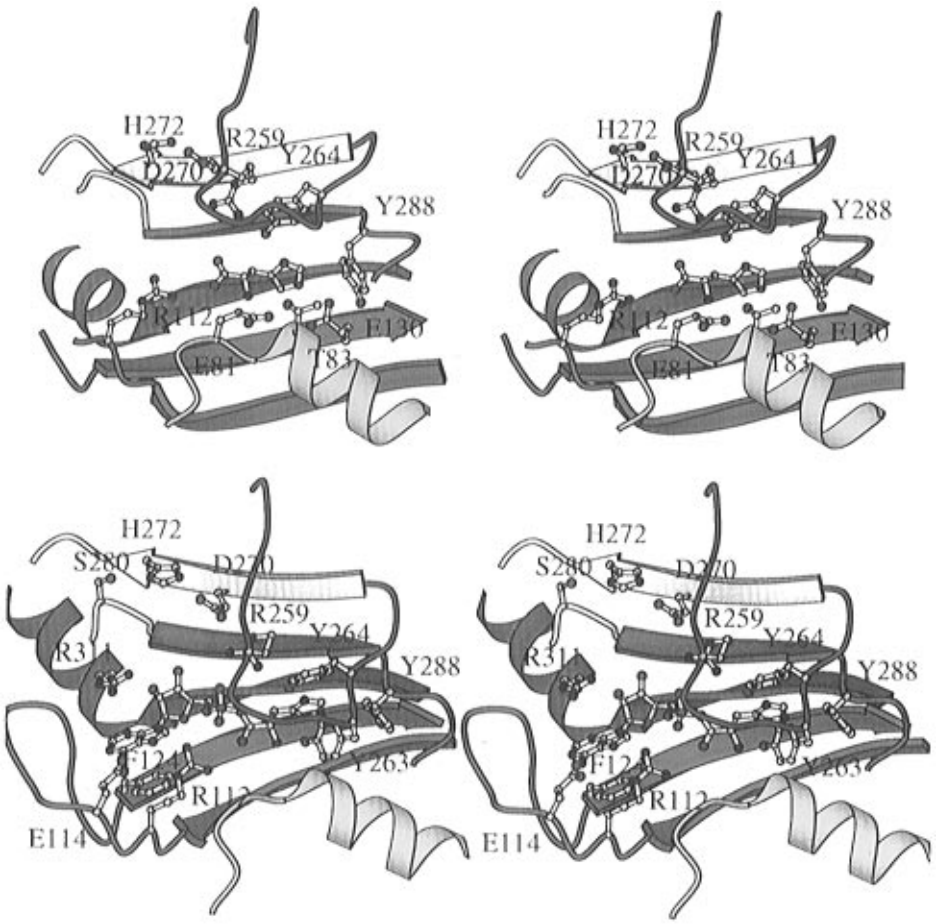

FIGURE 4: (a, top) Stereoview of active site residues interacting with the histidine. Motif 2 is in blue, motif 3 in red, the "TXE" loop in yellow, the histidine-1 loop in purple, and the histidine-2 strand/turn in green. Not all interacting residues (e.g., Tyr-263 is omitted) are shown for clarity. (b, bottom) Stereoview of active site residues interacting with the histidyl adenylate. Color scheme and comments as in (a).

described above, the C-terminal domain of one subunit packs entirely against the catalytic domain the other subunit. Figure 6 shows that after superposition of catalytic domins there are slight variations in the position of the C-terminal domain among the four independent monomers in the structure, involving largely rigid body movements with average RMS displacements of 0.86, 1.01, and 1.38 Å (respectively for the a, c, and d monomers, compared to the b monomer). The five-stranded mixed β-sheet has also been found in the C-terminal domain of the glycyl-tRNA synthetase (Logan *et al.*, 1995). However, in this enzyme the domain is differently orientated and packs against the catalytic domain of both subunits. The location of this domain with respect to the catalytic domain is analogous to the N-terminal anticodon binding domain of AspRS, strongly suggesting that it is involved in anticodon stem−loop binding and recognition (see Discussion). A search through the database of known structures using DEJAVU (G. Kleijwegt and A. Jones) did not identify any other protein domain with a similar fold. On the other hand, there are now known several other RNA binding domains of about 90 residues, such as the RNP, KH, and dsRBD, each of which has a slightly different α/β topology (Nagai, 1996).

Insertion Domain. Class II synthetases frequently possess a variable additional domain inserted into the catalytic domain between motifs 2 and 3 (Cusack *et al*., 1995), with the exception for the glycyl system where it is found between motifs 1 and 2 (Logan *et al*., 1995). In HisRSTT, we consider the insertion domain to be the 60 residues between 169 and 230. The following region from 231 to 264 is also specific to histidyl-tRNA synthetases but structurally forms part of the catalytic domain. The electron density for the insertion domain is in general weak, and the side chains have relatively high *B*-factors. Only in one of the four subunits could the chain be traced in the solvent-flattened MIR maps. It was not before the later stages in the refinement that the insertion domain for all subunits was included in the model since they do not satisfy the same noncrystallographic symmetry operators as the catalytic domain (Figure 6). It should be noted that this domain was completely disordered in the structure of HisRS from *E. coli* (Arnez *et al.*, 1995). The insertion domain consists of four α-helices (α6−9) which form a compact domain joined to the catalytic domain by a putative hinge formed by the close proximity of the ingoing and outgoing domain connections. The suggestion of a flexibily linked domain is reinforced by the narrow connection to the catalytic domain, the slightly different orientation in each subunit (Figure 6), and the fact that there are extremely few intimate contacts with the catalytic domain. The position of the insertion domain just above the active site strongly suggests that its function is to assist tRNA binding by clamping onto the acceptor stem of the tRNA (see Discussion).

The Histidyl Adenylate Complex. Two independent data sets to 3.2 Å have been collected on crystals which prior to freezing were soaked in 10 mM ATP and 10 mM Mn^{2+}

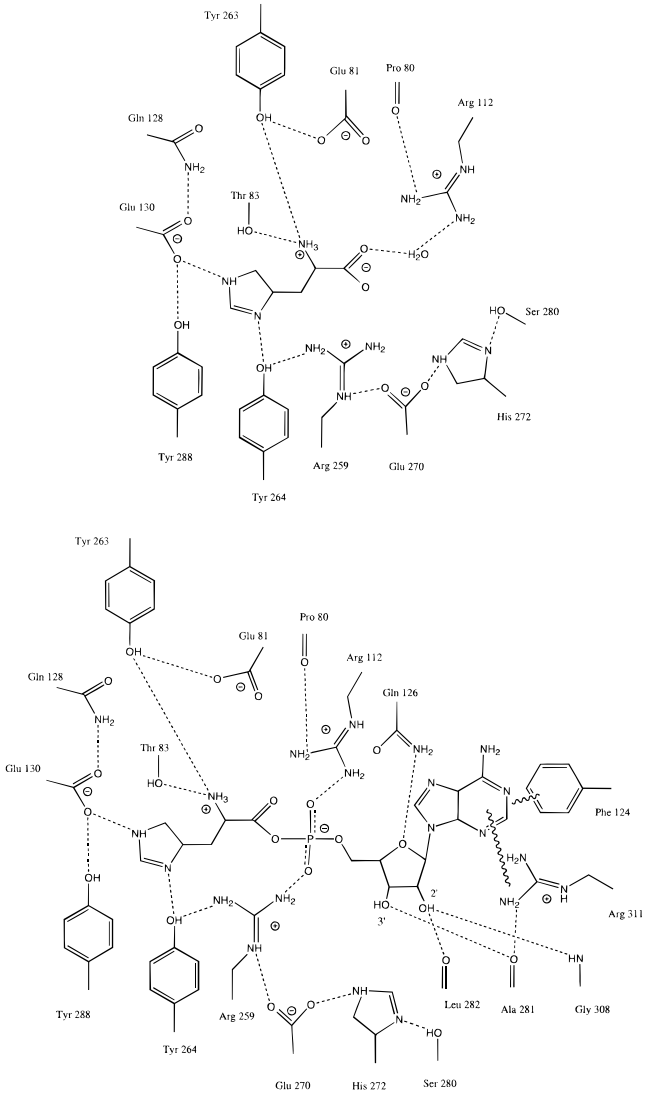

FIGURE 5: Schematic diagram showing hydrogen bond interactions of active site residues with (a, top) histidine and (b, bottom) histidyl adenylate. Putative hydrogen bonds are shown in dotted lines if the distance between the acceptor and donor is less than 3.2 Å. A wiggly line indicates stacking interactions.

(Table 1). The resolution and quality of these data are reduced compared to the native data due to the deterioration of the crystals upon soaking. Due to nonisomorphism the data sets could not be merged, but each data set individually leads to the same conclusions as described below. A difference Fourier map calculated using the accurate phases from the refined model of HisRS shows strong positive density in each active site into which a histidyl adenylate molecule can clearly be fitted, indicating that the activation reaction has occurred in the crystal (Figure 3b). The histidine binding pocket is essentially unchanged upon adenylate formation. On the other hand, as expected from results on other class II synthetases, there is an ordering of the motif 2 loop backbone (residues 115−120) into a β-hairpin conformation due to its main-chain interactions with the adenosine moiety of the adenylate which is stacked between the conserved motif 2 Phe-124 and motif 3 Arg-311. Consistently in each active site there is strong, elongated positive density, adjacent to the conserved motif 3 Arg-311 and Arg-120 of the motif 2 loop which is possibly residual pyrophosphate that has been produced by the activation reaction in the crystal (Figure 3b). There is no density that can be attributed to the divalent cation Mn^{2+} that was added with the ATP. Even at 3.2 Å resolution, this ion should be clearly visible were it still associated with the histidyl adenylate, as was found in the seryl adenylate case (Belrhali *et al*., 1995).

The detailed interactions with the histidyl adenylate are shown in Figures 4b and 5b, the interactions with the histidine moiety being essentially unchanged from those described above. Most significant is the fact that the α-phosphate of the histidyl adenylate is bound on each side by the motif 2 Arg-112 and the HisRS-specific Arg-259. The latter is in a position equivalent to that occupied by the divalent cation in the SerRS/ATP and SerRS/Ser adenylate complexes (Belrhali *et al*., 1995). On the other hand, the highly conserved glutamic acid residue that in most other class II synthetases binds the divalent cation and hydrogen bonds to the ribose O3′ (Belrhali *et al*., 1994, 1995) is absent in HisRS. This interaction is replaced by a putative hydrogen bond between the O3′ of the ribose and the carbonyl oxygen of Ala-281. There is also, as in the *E. coli* case, an extra hydrogen bond between the ribose O4′ and Gln-126, not found, for instance, in seryl-tRNA synthetase.

DISCUSSION

The crystal structure of HisRS from *T. thermophilus* complexed with either histidine and histidyl adenylate is very similar to that of *E. coli* complexed with histidyl adenylate (Arnez *et al*., 1995), but reveals in addition the fold of the insertion domain that was disordered in the case of *E. coli* HisRS. The structure confirms the crucial role of the HisRS-specific peptides 259-RGLDYY and 285-GGRYDG in forming a specificity pocket in which the substrate histidine is buried. The fact that both the *E. coli* (Francklyn *et al*., 1994) and *T. thermophilus* (Yaremchuk *et al*., 1995) enzymes require the presence of histidine for crystallization suggests that a conformational change occurs upon histidine binding, i.e., that the binding site might be formed by an induced-fit mechanism involving the stabilization of the histidine-1 peptide.

The structures presented above raise three interesting questions: (a) What is the mechanism of histidine activation? (b) How does the synthetase bind $tRNA^{His}$? (c) What conformational changes are associated with the overall aminoacylation reaction? Although the current structures do not answer these questions directly, they permit relevant observations to be made on each point.

(a) Mechanism of Histidine Activation. The first step in the overall aminoacylation reaction is activation of the amino acid by ATP leading to the aminoacyl adenylate, a stable enzyme-bound intermediate. This is generally believed to occur via an in-line displacement mechanism following nucleophilic attack by the carboxyl group of the amino acid on the α-phosphate of the ATP. Structure-based reaction mechanisms for activation have been described for both class I and class II synthetases (Perona *et al.*, 1993; Cavarelli *et al*., 1994; Belrhali *et al.*, 1995). For instance, for the seryl system the pentavalent transition state is proposed to be stabilized by the conserved motif II arginine, found in all class II synthetases, and a divalent cation (magnesium or manganese) bound between the α- and β-phosphates of the ATP and two protein ligands (Glu-345 and Ser-348 in SerRSTT). An equivalent divalent cation site cannot exist

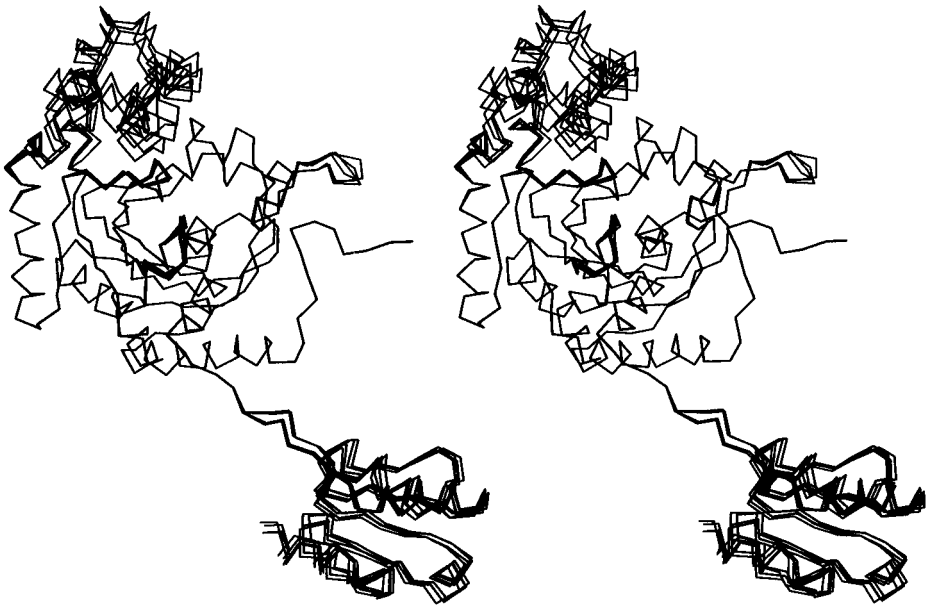

FIGURE 6: Superposition of the Cα traces of the four independent monomers in the crystallographic asymmetric unit, after using only the catalytic domains for alignment. Both the C-terminal and insertion domains have significant, largely rigid body displacements. For the C-terminal domains the average RMS (maximum) displacements are 1.01 (2.49), 1.38 (3.36), and 0.86 (1.25) Å, respectively, for the a, c, and d monomers, compared to the b monomer. For the insertion domains the average RMS (maximum) displacements are 1.96 (3.48), 2.62 (4.48), and 2.18 (3.59) Å, respectively, for the a, c, and d monomers, compared to the b monomer.

in HisRS since, first, the two protein ligands become respectively Ala-281 and Gly-284 in HisRSTT and, second, the guanidinium group of the HisRS-specific Arg-259 occupies virtually the same position as the divalent cation in SerRS. Arg-259 is close to the histidine carboxyl group or the α-phosphate of the histidyl adenylate in the two complexes described above. It is thus reasonable to propose that this residue plays a catalytic role in HisRS analogous to that proposed for the divalent cation in SerRS. Arg-259, together with the conserved motif 2 Arg-112, would thus be responsible for initial neutralization of the negative charge of the histidine carboxyl group and stabilization of the doubly charged pentavalent transition state. There is no electron density that can be unambiguously assigned to a divalent cation, which might for instance correspond to either of the two additional ions on either side of the β- and γ-phosphates that are observed in the SerRSTT−ATP complex (Belrhali *et al*., 1995). Higher resolution data on a complex with ATP or an ATP analogue and divalent cations would be required to confirm the location or absence of any divalent cation binding site. Magnesium is required for the overall histidine aminoacylation reaction in HisRSTT (A. Yaremchuk, unpublished results) although its importance for the activation step has not yet been studied.

These results show that although the arrangement of the ATP and amino acid substrates is essentially the same in the three class II synthetase active sites for which structural data exit (AspRS, Cavarelli *et al*., 1994; SerRS, Belrhali *et al*., 1995; and HisRS), they differ in the manner in which extra positive charge is provided close to the catalytic center.

(b) tRNA Binding. Figure 7a shows the electrostatic potential of the dimer. An extended positive potential surface running diagonally from the active site to the C-terminal domain of the same monomer can be seen which could be important in recognizing the negatively charged tRNA backbone. Using structural knowledge of the mode of binding of cognate tRNA to yeast AspRS (Ruff *et al*., 1991) and SerRSTT (Cusack *et al*., 1996) we have modeled a tRNA molecule docked to the HisRSTT dimer (Figure 7b), an excercise also carried out in the case of *E. coli* HisRS (Arnez *et al*., 1995). Despite the obvious limitations in such a docking model, a number of points can be made. First, based on the consistent orientation with which tRNAs enter the class II active site, and the fact that the C-terminal domain of HisRS occupies the same spatial position as the N-terminal domain of yeast AspRS, it is evident that the $tRNA^{His}$ will bind with its anticodon stem−loop in contact with the C-terminal domain of the same subunit as where the 3′ end enters the active site, in agreement with the electrostatic potential surface. While the bulk of the interactions of the tRNA would thus be with the same HisRS subunit, the docking model suggests that the loop 96−98 from the *other* subunit could interact with the tRNA in the region of nucleotides 10−11. As suggested by the electrostatic surface, there are a large number of conserved basic residues that could contact tRNA backbone phosphates. The docking model suggests in particular that the insertion domain residues Arg-204, Arg-197, and Lys-209, conserved in all prokaryotic HisRSs (Figure 1), are well positioned to interact with phosphates 73−75 on the 3′ strand backbone. Also the absolutely conserved residue Arg-7 (from the N-terminal strand which packs on the other subunit), together with Arg-74′ (on the other subunit), could interact with the tRNA backbone in the region of P67. These putative backbone interactions would help to explain the strong binding of acceptor stem minihelices to HisRS (Francklyn *et al*., 1992). Most interesting is the question of which elements are responsible for the specific recognition of the critical additional G-1·C73 base pair. As with other class II synthetases (Cusack et al., 1996), the variable motif 2 loop (115-RPQK in HisRSTT) is most likely interacting inside the major groove of the tRNA acceptor stem, with Gln-117, conserved in all prokaryotic HisRS, being well placed to make base-specific contacts with G-1·C73 or G1·C72. In addition, as also proposed by Arnez *et al*. (1995), the loop between β9 and β10 containing Gln-269, which is reasonably

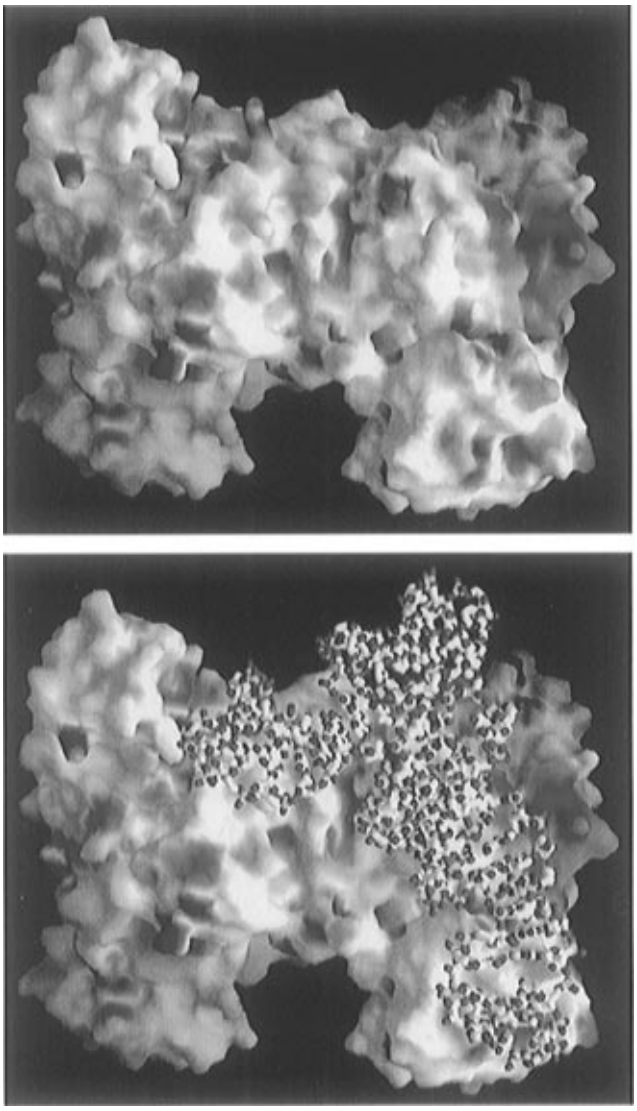

FIGURE 7: (a, top) GRASP (Nicholls *et al*., 1991) view of the electrostatic potential surface around HisRSTT and (b, bottom) view with the superposed docked tRNA molecule. Negative potential (−12 kT) is in red and positive (12 kT) in blue.

well ordered in the HisRSTT structure, could also interact with C73. Finally, there are three largely conserved basic residues, Lys-63, Arg-71, and Arg-115, that are strategically positioned to possibly make contacts with the extra 5′-phosphate of G-1. The fact that Lys-63 is absolutely conserved in all known HisRS sequences makes it a particularly plausible candidate for this important interaction.

Concerning the mode of binding of the C-terminal domain to the anticodon stem−loop of $tRNA^{His}$, this is an outstanding question that can only be satisfactorily addressed by a crystal structure of the cognate complex. Interestingly, there are extremely few conserved residues in the C-terminal domain which could give a hint as to the critical regions. This applies not only to known HisRS sequences (Figure 1) which generally will recognize a GUG anticodon but also to other class IIa synthetases which possess this domain (Cusack, 1993). This is in contrast to the three class IIb synthetases whose homologous N-terminal domains all recognize a central U-35 in the anticodon by means of absolutely conserved glutamine and phenylalanine residues (Cavarelli *et al*., 1993; Cusack *et al*., 1996b). However, as has been remarked above, the first part of the C-terminal domain is largely involved in the interface to the catalytic domain of the other subunit. This is consistent with the docking model which suggests that it is the second half of the C-terminal domain that could interact best with the tRNA. In particular, the helix α14 is in a position to bind to the anticodon stem−loop from the major groove side, and exposed residues on strands β14 (e.g., Phe-383), β15 (e.g., Lys-397), and β16 (e.g., Gln-404) could interact with the anticodon loop nucleotides. It is interesting to note that, in HisRSTT, Phe-383 and Gln-404 are juxtaposed in a very similar way to the conserved glutamine and phenylalanine that interact with U-35 in class IIb synthetases [see Cusack *et al*. (1996b)].

(c) Role of the Insertion Domain and the Dynamics of Aminoacylation. The insertion domain is poised over the active site in a way that it could clamp onto the tRNA. Basic residues Arg197, Arg204, and Lys209 as well as Asp-207, conserved in all prokaryotic HisRSs, are pointing toward the active site, making it possible for them to interact with the 3′ strand backbone of the tRNA acceptor stem (see above). Furthermore, a slight movement of the insertion domain toward the active site would allow good van der Waals contact between otherwise exposed hydrophobic residues Met-203 and Met-225 in the insertion domain and the conserved Val-258 in the critical histidine-1 peptide as well as complementary electrostatic interactions between charged residues on the insertion domain (e.g., Arg-172 and Glu-196) with catalytic domain residues (e.g., Asp-262 on the histidine-1 peptide or Asp-59 and Arg-62 in α3). Some of these interactions are seen in the four different monomers in the crystallographic asymmetric unit due to the slightly different positions of the insertion domain. The putative closing of the insertion domain over the tRNA poses a serious problem about what triggers the release of the histidyl-tRNA, since the histidine would be essentially deeply buried within the active site. In this connection it should be mentioned that modeling the 3′ end of the tRNA into the active site of the histidyl adenylate complex can be done satisfactorily, placing the 3′-OH of ribose-76 adjacent to the carbonyl group of the adenylate. However, the space available for the A-76 base is rather limited although it probably fits into a hydrophobic pocket formed by conserved hydrophobic residues in the region of helices α2 and α3 (e.g., Phe-50, Val-54, Ile-60, and Met-65 as well as Pro-80; see Figure 1). Note that this is the same conserved region containing charged residues that could also interact with the insertion domain (see above). These observations suggest that either tRNA binding or the completion of the aminoacylation reaction should lead to significant conformational rearrangement in the active site. A possible hypothesis is that concomitant binding of the tRNA and closing of the insertion domain could lead to new interactions between the insertion domain and both the histidine-1 peptide and the highly conserved region around residue 60. Resultant conformational adjustments of these regions could open up slightly the active site to permit binding of A-76 and subsequent release of the histidine moiety of the charged $tRNA^{his}$ after the aminoacylation step. However, it should be borne in mind that the conformational changes may in fact be larger scale and also involve the C-terminal anticodon binding domain, consistent with the small flexibility seen in this domain (Figure 6) and with a recent report that mutations in this domain and its interface with the catalytic domain can

compensate for unfavorable mutations in the $tRNA^{His}$ discriminator base (Yan *et al*., 1996).

The conformational dynamics during the overall aminoacylation reaction is clearly a subtle and important element in the functioning and specificity of aminoacyl-tRNA synthetases as has been demonstrated recently in the case of seryl-tRNA synthetase (Cusack *et al*., 1996a). In the case of histidyl-tRNA synthetase it is evident that further understanding will depend on the structure determination of the complex between HisRS, histidine, and $tRNA^{His}$ (Yaremchuk *et al*., 1995).

ACKNOWLEDGMENT

We thank Michael Wulff (ESRF) for help with the measurements on ID13. Molscript (Kraulis, 1994) was used for Figures 2, 4, and 6.

REFERENCES

Arnez, J. G., Harris, D. C., Mitschler, A., Rees, B., Francklyn, C. S., & Moras, D. (1995) *EMBO J. 14*, 4143−4155.

Artymiuk, P. J., Rice, D. W., Poirrette, A. R., & Willett, P. (1994) *Nat. Struct. Biol. 1*, 758−760.

Belrhali, H., Yaremchuk, A. D., Tukalo, M. A., Larsen, K., Berthet-Colominas, C., Leberman, R., Beijer, B., Sproat, B., Als-Nielsen, J., Grübel, G., Legrand, J.-F., Lehmann, M., & Cusack, S. (1994) *Science 263*, 1432−1436.

Belrhali, H., Yaremchuk, A., Tukalo, M., Berthet-Colominas, C., Rasmussen, B., Bösecke, P., Diat, O., & Cusack, S. (1995) *Structure 3*, 341−352.

Biou, V., Yaremchuk, A., Tukalo, M., & Cusack, S. (1994) *Science 263*, 1404−1410.

Brick, P., Bhat, T. N., & Blow, D. M. (1989) *J. Mol. Biol. 208*, 83−98.

Brünger, T. A. (1992) *X-PLOR version 3.1*, Yale University Press, New Haven, CT.

Brunie, S., Zelwer, C., & Risler, J. L. (1990) *J. Mol. Biol. 216*, 411−424.

Cavarelli, J., Rees, B., Ruff, M., Thierry, J.-C., & Moras, D. (1993) *Nature 362*, 181−184.

Cavarelli, J., Eriani, G., Rees, B., Ruff, M., Boeglin, M., Mitschler, A., Martin, F., Gangloff, J., Thierry, J-C., & Moras, D. (1994) *EMBO J. 13*, 327−337.

Collaborative Computational Project Number 4 (1994) The CCP4 Suite: Programs for Protein Crystallography, *Acta Crystallogr. D50*, 760−763.

Cusack, S. (1993) *Biochimie 75*, 1077−1081.

Cusack, S. (1995) *Nat. Struct. Biol. 2*, 824−831.

Cusack, S., Yaremchuk, A., & Tukalo, M. (1996a) *EMBO J. 15*, 2834−2842.

Cusack, S., Yaremchuk, A., & Tukalo, M. (1996b) *EMBO J. 15*, 6321−6334.

Delarue, M. (1995) *Curr. Opin. Struct. Biol. 5*, 48−55.

Delarue, M., Poterzman, A., Nikonov, S., Garber, M., Moras, D., & Thierry, J. C. (1994) *EMBO J. 13*, 3219−3229.

Doublié, S., Bricogne, G., Gilmore, C., & Carter, C. W., Jr. (1995) *Structure 3*, 17−31.

Engh, R. A., & Huber, R. (1991) *Acta Crystallogr. A47*, 392−400.

Eriani, G., Delarue, M., Poch, O., Gangloff, J., & Moras, D. (1990) *Nature 347*, 203−206.

Eriani, G., Cavarelli, J., Martin, F., Dirheimer, G., Moras, D., & Gangloff, J. (1993) *Proc. Natl. Acad. Sci. U.S.A. 90*, 10816−10820.

Francklyn, C., & Schimmel, P. (1990) *Proc. Natl. Acad. Sci. U.S.A. 87*, 8655−8659.

Francklyn, C., Shi, J.-P., & Schimmel, P. (1992) *Science 255*, 1121−1125.

Francklyn, C., Harris, D., & Moras, D. (1994) *J. Mol. Biol. 241*, 275−277.

Fujinaga, M., Berthet-Colominas, C., Yaremchuk, A. D., Tukalo, M. A., & Cusack, S. (1993) *J. Mol. Biol. 234*, 222−233.

Himeno, H., Hasegawa, T., Ueda, T., Watanabe, K., Miura, K., & Shimizu, M. (1989) *Nucleic Acids Res. 19*, 7855−7863.

Jones, A. T., Cowan, S. W., Zou, J.-Y., & Kjeldgaard, M. (1991) *Acta Crystallogr. A47*, 110−119.

Kabsch, W., & Sander, C. (1983) *Bioploymers 22*, 2577−2637.

Kraulis, P. J. (1991) *J. Appl. Crystallogr. 24*, 946−950.

Leslie, A. G. W. (1992) *Joint CCP4 and ESF-EACBM Newsletter on Protein Crystallography*, No. 26, Daresbury Laboratory, Warrington WA4 4AD, England.

Logan, D. T., Mazauric, M.-H., Kern, D., & Moras, D. (1995) *EMBO J. 14*, 4156−4167.

Mosyak, L., Reshetnikova, L., Goldgur, Y., Delarue, M., & Safro, M. G. (1995) *Nat. Struct. Biol. 2*, 537−547.

Nagai, K. (1996) *Curr. Opin. Struct. Biol. 6*, 53−61.

Nameki, N., Asahara, H., Shimizu, M., Okada, N., & Himeno, H. (1995) *Nucleic Acid Res. 23*, 389−394.

Nicholls, A., Sharp, K. A., & Honig, B. (1991) *Proteins 11*, 281−286.

Nureki, O., *et al.* (1995) *Science 267*, 1958−1965.

Onesti, S., Miller, A. D., & Brick, P. (1995) *Structure 3*, 163−176.

Otwinowski, Z. (1993) in *Data Collection and Processing* (Sawey, L., Isaacs, N., & Burley, S., Eds.) pp 56−62, SERC Daresbury Laboratory, Washington, U.K.

Perona, J. J., Rould, M. A., & Steitz, T. A. (1993) *Biochemistry 32*, 8758−8771.

Poterszman, A., Delarue, M., Thierry, J.-C., & Moras, D. (1994) *J. Mol. Biol. 244*, 158−167.

Rould, M. A., Perona, J. J., Soll, D., & Steitz, T. A. (1989) *Science 246*, 1135−1142.

Ruff, M., Krishnaswamy, S., Boeglin, M., Poterzman, A., Mitschler, A., Podjarny, A., Rees, B., Thhierry, J. C., & Moras, D. (1991) *Science 252*, 1682−1689.

Sanger, F., Nicklen, S., & Coulson, A. R. (1977) *Proc. Natl. Acad. Sci. U.S.A. 74*, 5463−5467.

Steinberg, S., Misch, A., & Sprinzl, M. (1993) *Nucleic Acids Res. 21*, 3011−3015.

Wek, R. C., Jackson, B. M., & Hinnebusch, A. G. (1989) *Proc. Natl. Acad. Sci. U.S.A. 86*, 4479−4583.

Yan, W., & Francklyn, C. (1994) *J. Biol. Chem. 269*, 10022−10027.

Yan, W., Augustine, J., & Francklyn, C. (1996) *Biochemistry 35*, 6559−6585.

Yaremchuk, A. D., Cusack, S., Åberg, A. Gudzera, O., & Tukalo, M. (1995) *Proteins 22*, 426−428.

BI9618373